Evaluating the Retreat, Stabilization, and Regrowth of Crane Glacier against Marine Ice Cliff Process Models

C. Needell[1] and N. Holschuh[1]

[1]Department of Geology, Amherst College, Amherst, MA, USA

Contents of this file

Introduction

The following text, figures, and their associated captions supplement the main text of "Evaluating the Retreat, Stabilization, and Regrowth of Crane Glacier against Marine Ice Cliff Process Models."

Text S1:

We relied on the following information from referenced papers for the cliff-height failure criteria presented in Figure 3. Below, we deconstruct our classification of "strong" and "weak" ice, and our choice of "best estimate" cliff height values.

Ultee and Bassis, 2016

The authors present a function (Eq. 26 from Ultee and Bassis) that relates terminus ice thickness and water depth, which we use to reproduce their Fig. 1 (see Figure S6). We extend their Fig. 1 to depths > 1000 m (suitable for depths near the Crane terminus, where water depth was near 900 m) and solve for the subaerial cliff height (H – D) at 900 m water depth for each yield strength (Fig. S6).

The authors test their model using what they deem to be realistic yield strengths of 50 – 300 kPa, selecting 150 kPa as a best fit value to reproduce retreat of Columbia Glacier (p. 1146). Here we present cliff height threshold values for 50 kPa as a weak case, 300 kPa as a strong case, and 150 kPa as the model best estimate.

Parizek et al., 2019
The abstract states that "the threshold cliff height for slumping is likely slightly above 100 m in many cases, and roughly twice that (145–285 m) in mechanically competent ice under well-drained or low-melt conditions" (449).

Following from this statement, we use 100 m as the critical cliff height for damaged ice, and use 145-285 m as the critical height range for strong ice. We choose the 100 m threshold as the model best estimate, because it is presented in the referenced work as consistent with observed slumping events and as the threshold "in many cases" (Abstract from Parizek et al.).

Bassis et al., 2021
In addition to the cliff height failure threshold, we also present criteria for the bed slope and ice thickness gradient, which are thought to define the threshold for unstable retreat. Because the exact failure thresholds for bed slope and ice thickness gradient are not directly stated in the manuscript, we derive the criteria presented in Figure 3 of our work from Figure 4 from Bassis et al., which shows the "average rate of terminus advance over 1 year for an initial 800-m-thick glacier terminating in 690 m of water [therefore a 110 m subaerial cliff height] for a range of thickness gradients and upstream velocities" (p. 3) and displays the "catastrophic collapse" (p. 3) zone given a particular bed slope, ice thickness gradient, and inflow velocity. Based on Figure 4, we approximated the criteria required for catastrophic collapse.

We consider this critical height representative of damaged ice, because the Bassis et al. (2021) supplement states that their "estimate of the yield strength implies the presence of starter cracks that are tens of centimeters long," and that "the assumption that ice is undamaged results in significantly stronger ice and a much larger inferred ice strength," which results in "cliffs [that] are stable to a much greater height than obtained from our simulations" (S1.1.6).

Bassis and Walker, 2012, and Bassis and Ultee, 2019
In equation 2.12, Bassis and Walker (2012) derive an upper bound on ice thickness at the terminus of glaciers that depends primarily on two things: crevasse penetration and the depth-integrated yield strength of ice (which they define as 1 MPa). Bassis and Ultee (2019) showed a missing factor of 2 in the derivation presented in Bassis and Walker, and re-derive the equation for their model of calving glaciers, which they

present in equation 48 of their paper. Using equation 48 and a water depth of 900 m, we calculate 3 possible threshold cliff heights for Crane: cliff heights in ice with no crevassing (r=0, strong), in ice with crevasse penetration consistent with a Nye zero-stress model at floatation (r=0.5, best estimate), and in ice with the greatest crevasse penetration while still allowing an ice thickness greater than the buoyancy thickness (r=0.7, weak). See Figure S7 for the results.

Crawford et al., 2021

Crawford et al. state that "structural ice-cliff failure is observed for B_n [normal basal slip] conditions when $H_c \geq 136$ m" (p. 2).

We consider this cliff height representative of strong ice, because the manuscript states that "this retreat rate parameterization was derived for simulations of largely undamaged ice with high fracture toughness," (p. 6) and from information given in the supplement: "We note here that our main simulation series, which underpins the ice-cliff failure retreat rate parameterization development, is conducted with the standard HiDEM structure and parameter settings. As noted in the main text, the HiDEM lattice structure and yield strength combine to represent strong ice that is largely undamaged when initialized with the standard percentage of pre-seeded broken bonds" (Supplementary Note 1 from Crawford et al.).

Clerc et al., 2019

Clerc et al. state that "as the ice-shelf removal timescale increases, viscous relaxation dominates, and the critical height increases to ~540 m for timescales greater than days" (p. 12,108). Also see Figure 4 from Clerc et al. for a plot of cliff height compared to timescale of ice shelf collapse, which shows that a critical height of ~540 m is required for a 10^1-days timescale of ice shelf collapse (the duration of the Larsen B Ice Shelf Collapse). It is unclear how one should treat the characteristic timescale of a single calving event (it could be seconds to minutes), but using small values for Δt in the Clerc et al. framework would result in effectively no stable ice cliffs, which is inconsistent with the retreat pattern we see at Crane.

We treat this 540 m critical height as representing strong ice, given the following statement: "our prediction that a cliff formed at the grounding line could be stable at great (~540 m) heights assumes the ice is undamaged," (p. 12,115) and their 60 m critical height as representing damaged ice, given: "prescribing a fracture toughness of 50 kPa m1/2 and crack half-length of 50 mm (values chosen for damaged ice at calving fronts by Parizek et al., 2019) yields a 60-m critical height" (p. 12,115). The authors state that they "predict cliff failure only initiates in cliffs taller than ~540 m," (p. 12,115) the cliff height consistent with undamaged ice; thus, we treat 540 m as their model best estimate.
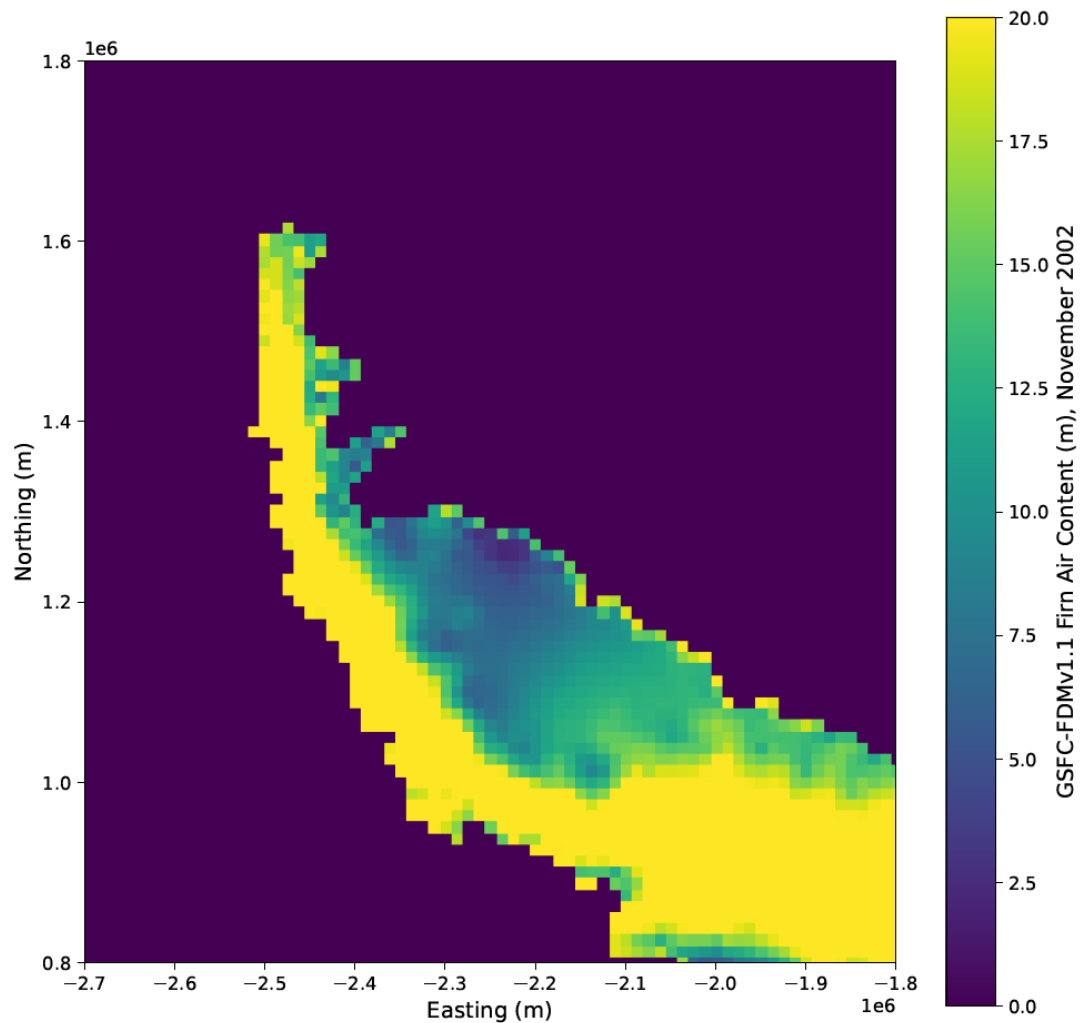
Figure S1. Modeled Firn Air Content (FAC) of the Antarctic Peninsula from November, 2002 (Medley et al., 2020). Firn Model Resolution is 10 km by 10 km. FAC estimates for the Larsen C Ice Shelf closely agree with observations from this period (Ashmore et al., 2017), which supports an interpretation of 10+ m of FAC along the main trunk of Crane Glacier. If included in the analysis, maximum cliff heights at Crane are reduced to 95 m, below the threshold for failure in all models but Clerc et al. (2019) and Ultee and Bassis (2016), when damaged ice is used.
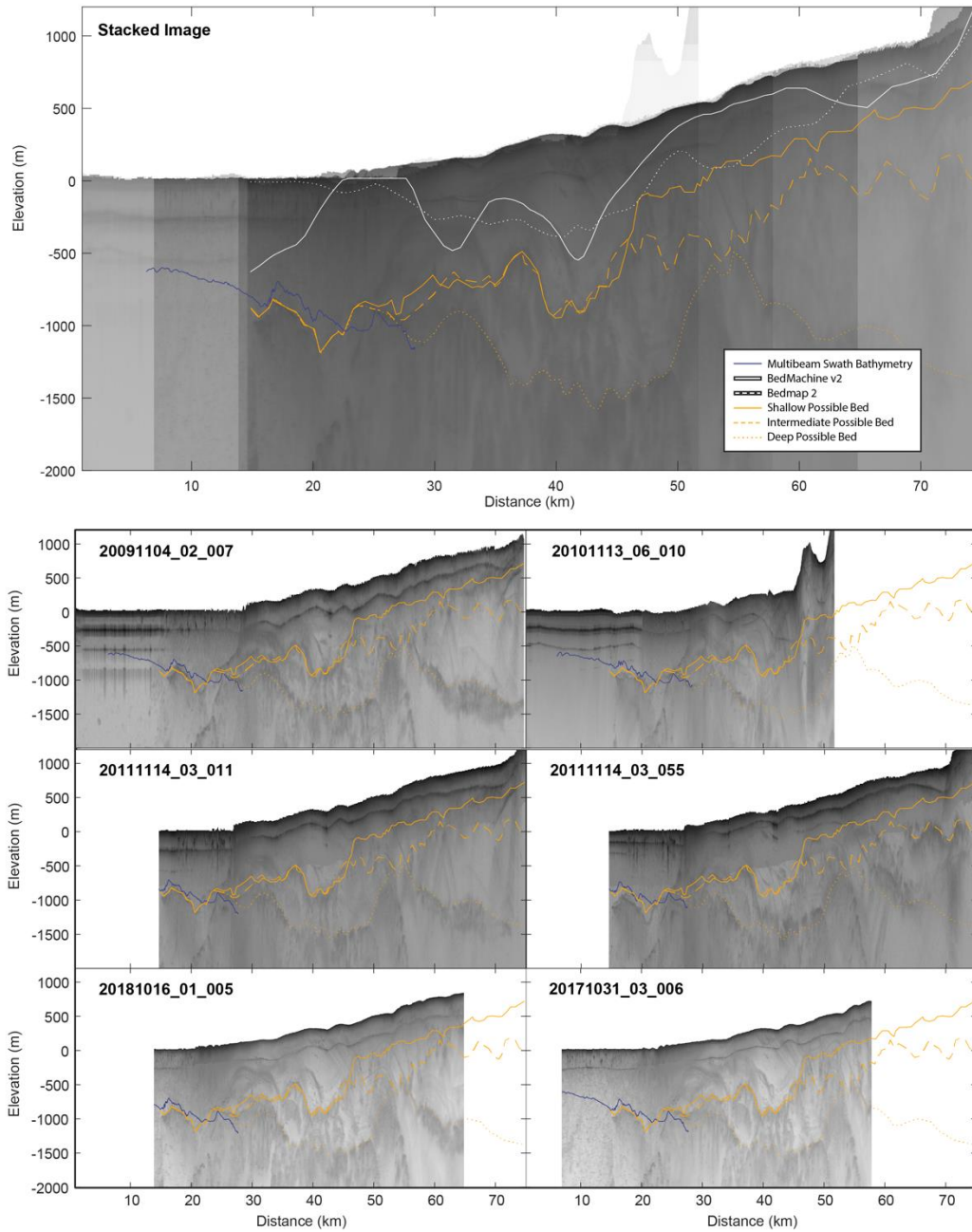
4

Figure S2. Radar imagery collected along the main trunk of Crane Glacier. Because of the narrow fjords and complex topography of the Antarctic Peninsula, those data suffer from significant off-axis clutter (primarily valley side walls), resulting in an ambiguous basal reflector and an unknown ice thickness profile. In 2017, the central flowline of Crane Glacier was resurveyed, but this time with NASA's P3 aircraft equipped with a

fuselage and wing antenna array. While this system should allow for direction of arrival analysis that reduces the ambiguity of the bed reflector, the low signal-to-noise ratio in the data prevents swath radar processing. Instead, we use the stack of all available radar data, compared with the multibeam swath bathymetry, to derive a range of reasonable bed elevations, with the shallow bed thought to be the most plausible. All realistic beds are significantly deeper (500+ meters) than established continent wide bed topography products.
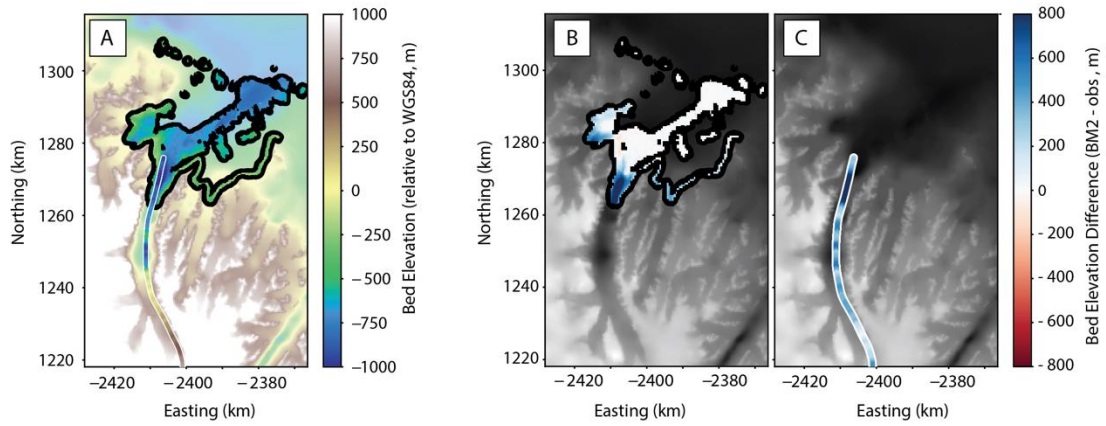
Figure S3. Maps showing the (a) bathymetry in the fjord and along the main trunk of Crane Glacier (derived from radar data in Fig. S3), and (b) and (c) the difference between the bed elevations from Rebesco et al. (2014), this study, and BedMachine Antarctica v2. Positive elevation differences indicate regions where BedMachine Antarctica's bed elevation is high relative to observations. Height differences presented in S3c can be seen in Figure S2 by comparing the solid white and solid orange curves.
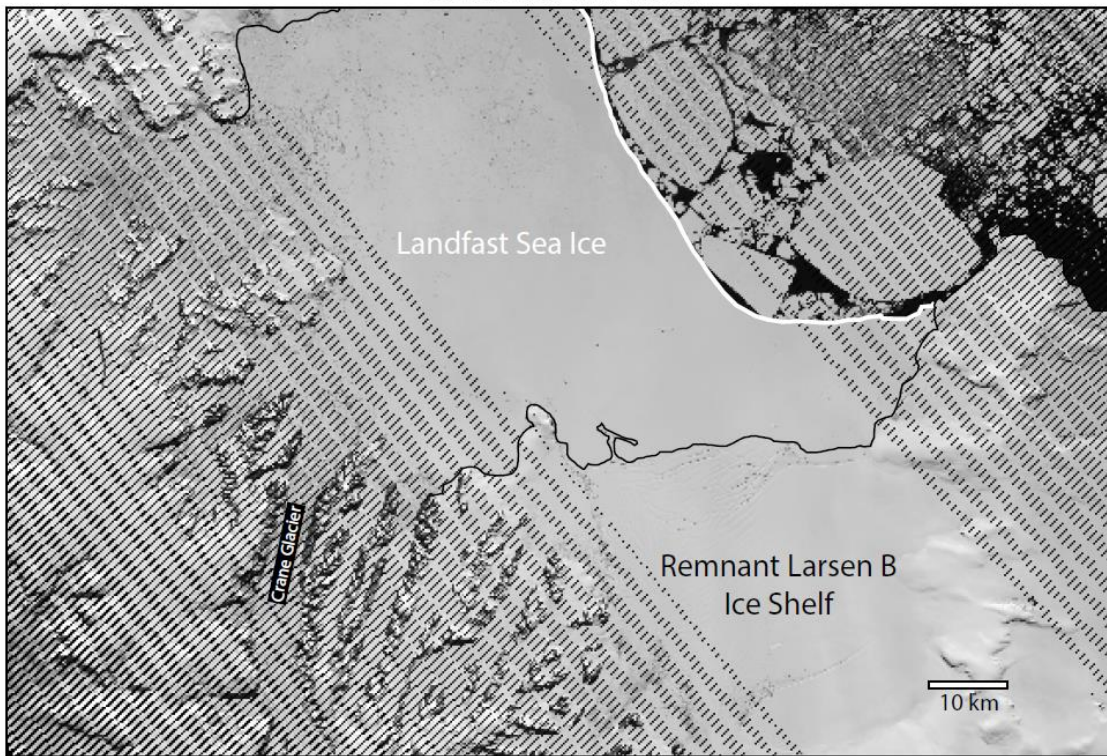
Figure S4. Landsat image of the Larsen B Embayment from December 27th, 2011. This image captures the landfast sea ice that established itself in front of Crane Glacier, which likely provided sufficient buttressing stress to enable the regrowth of a floating ice shelf at Crane.
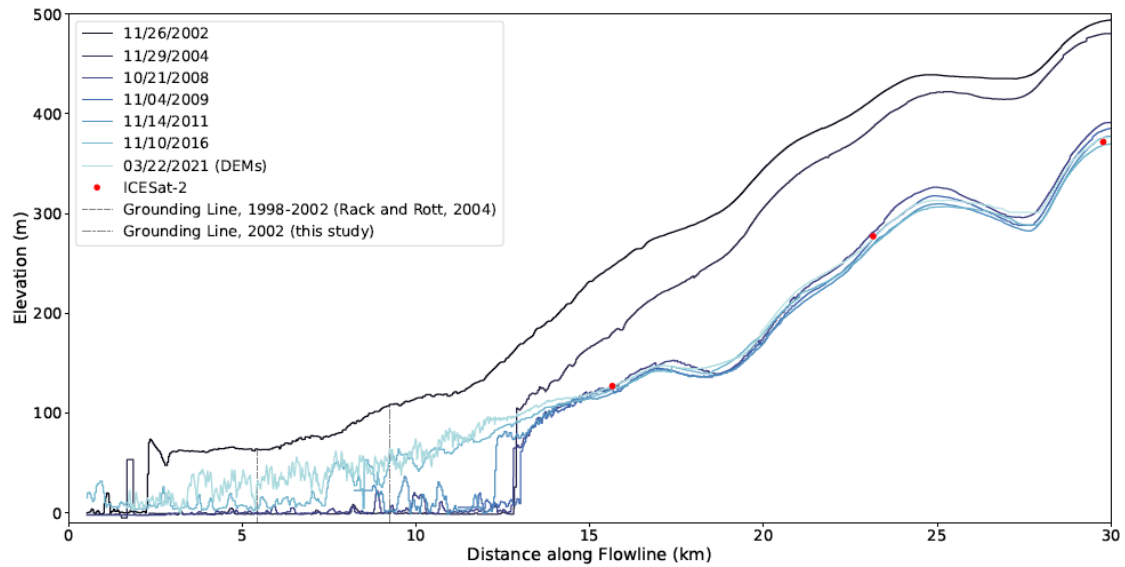
Figure S5. Extended surface elevation profile, capturing evidence of upstream elevation change. Local thickening upstream of the 2021 glacier terminus occurred ~12 km along the flowline from 2008-2021, and a period of thinning 12-30 km along the flowline occurred from 2002-2008. Data represent a combination of NASA airborne altimetry data (Airborne Topographic Mapper data and Land, Vegetation, and Ice Sensor data), and ICESat-2 calibrated stereophotogrammetric DEMs.

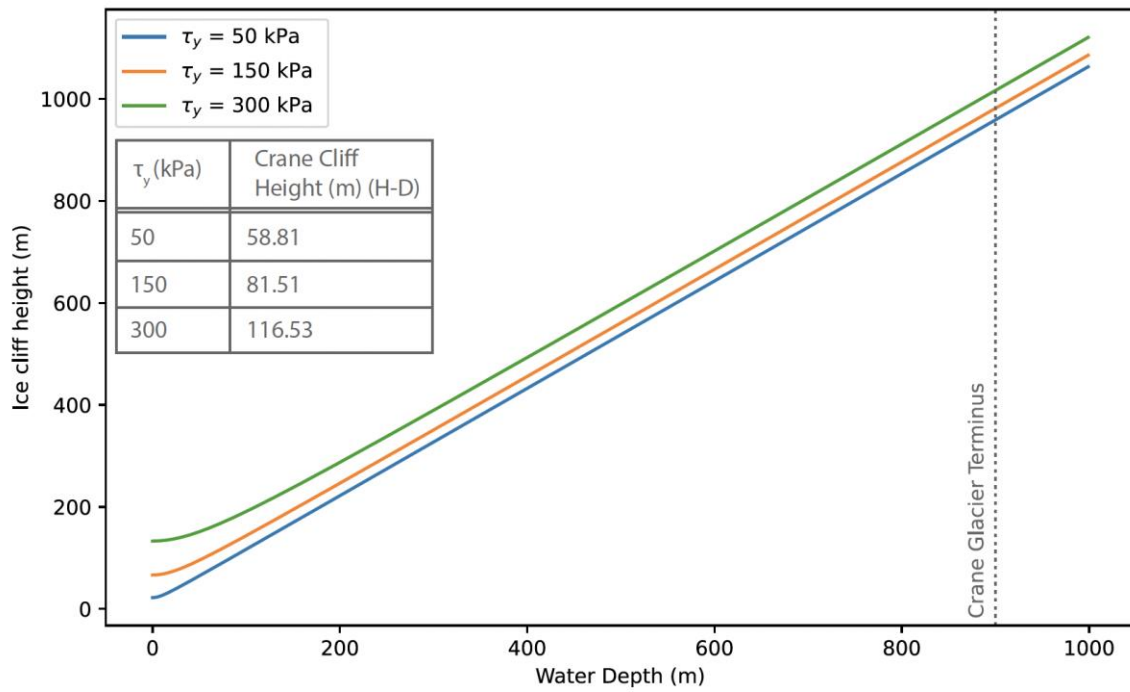| τ_y (kPa)	Crane Cliff Height (m) (H-D)
50	58.81
150	81.51
300	116.53

Figure S6: Cliff Failure Criteria from Ultee and Bassis (2016). Here we extend Figure 1 from Ultee and Bassis (2016) to capture water depths consistent with the Crane terminus in 2002. From these curves, we derive the critical cliff height at Crane for yield strengths of 50, 150 and 300 kPa.
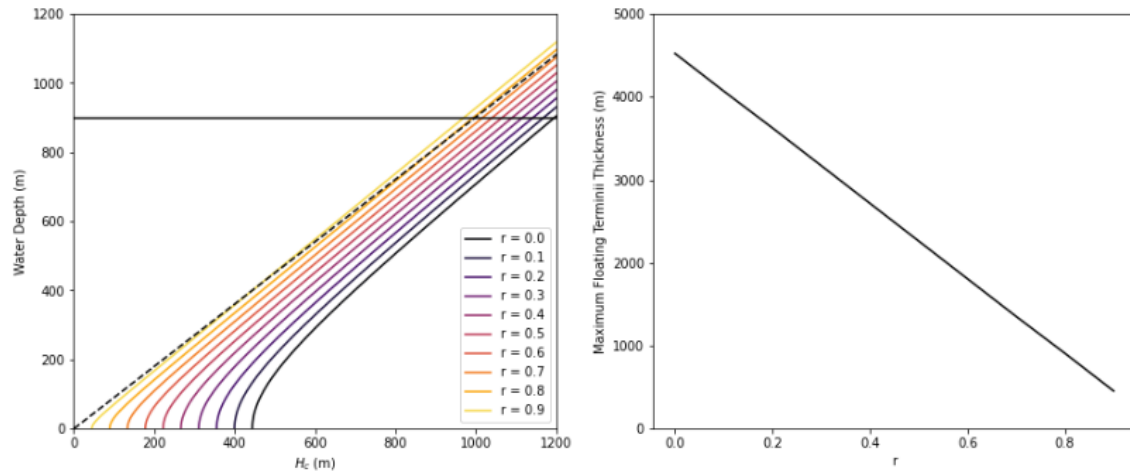
Figure S7: Reproduction of Figure 3 from Bassis and Walker (2012) using the updated derivation from Bassis and Ultee (2019). H_c is the maximum stable ice thickness and r is the crevasse penetration ratio (where 0 is no crevassing, 1 is full-thickness crevassing). The dashed black line represents the floatation thickness for a given water depth. We include a horizontal line indicating the water depth at Crane Glacier, which we use to calculate the range of reasonable cliff heights for Figure 3 in the main text of this manuscript.